IEEE Access
Multidisciplinary ⋮ Rapid Review ⋮ Open Access Journal

Received 6 February 2023, accepted 19 February 2023, date of publication 1 March 2023, date of current version 13 March 2023.

Digital Object Identifier 10.1109/ACCESS.2023.3251220

RESEARCH ARTICLE

Growth Pattern Fingerprinting for Automatic Analysis of Lung Adenocarcinoma Overall Survival

NAJAH ALSUBAIE[1], SHAN E. AHMED RAZA[2], DAVID SNEAD[3], AND NASIR M. RAJPOOT[2], (Senior Member, IEEE)

[1]Department of Computer Sciences, College of Computer and Information Sciences, Princess Nourah bint Abdulrahman University, Riyadh 11671, Saudi Arabia
[2]Department of Computer Science, The University of Warwick, CV4 7AL Coventry, U.K.
[3]Department of Histopathology, University Hospitals Coventry and Warwickshire (UHCW), CV2 2DX Coventry, U.K.

Corresponding author: Najah Alsubaie (nmoalsubaie@pnu.edu.sa)

This research was funded by Princess Nourah bint Abdulrahman University Researchers Supporting Project number (PNURSP2023R321), Princess Nourah bint Abdulrahman University, Riyadh, Saudi Arabia.

This work involved human subjects or animals in its research. Approval of all ethical and experimental procedures and protocols was granted by the National Research Ethics Service North West REC under Reference No. 15/NW/0843.

ABSTRACT Lung adenocarcinoma (LUAD) tumour tissue grows into variable morphological architecture called growth patterns (GPs). The GPs are clinically linked to the biological behaviour of the tumour. However, due to the complex heterogeneity of the tumours, there is high inter-and intra-observer variability in the pathologist reporting of GPs. This paper proposes a deep-learning model for automatically classifying the LUAD growth patterns in whole slide images (WSIs). The model is trained and tested on 78 cases of LUAD in the digitised WSI of the sample. For each case, all the growth patterns were automatically classified and quantified. Our multivariate analysis shows that lepidic and micropapillary patterns are independent predictors for five-year survival ($p<0.05$). The proposed model splits our study cohort into short- and long-term survival with $p=0.009$.

INDEX TERMS Digital pathology, machine learning, deep learning, whole-slide image, growth pattern, survival analysis.

I. INTRODUCTION

Identifying LUAD growth patterns is critical for the diagnosis and prognosis of lung cancer. Growth patterns have variable textures, shapes, and sizes. They could appear individually or fused into each other, which makes it challenging to avoid inter-and intra-observer variability. Tumour growth patterns (also referred to as adenocarcinoma histology subtypes) are some of the main histological characteristics that distinguish LUAD from the other types of non-small cell lung carcinomas (NSCLC), such as lung squamous carcinoma [1], [2]. A growth pattern is a pattern the tissue makes when it grows into a specific morphological architecture. Growth patterns are clinically linked with the biological behaviour of the tumour. According to the latest 2015 WHO classification of lung tumours [3], LUAD has five growth patterns: acinar, papillary, micropapillary, solid and lepidic. Figure 1 shows examples of these patterns. The acinar pattern is identified by glandular formation containing columnar-shaped tumour cells forming acini and tubules. A solid tumour is identified as sheets or nests of tumour cells. The lepidic pattern is composed of neoplastic cells growing along the alveolar walls. It often has no architectural complexity and does not contain the stromal, vascular, or lymphatic invasion. The papillary pattern is identified by the papillary structure with fibrovascular cores that replace the alveolar. At least one blood vessel can be observed within the papillary structure. Psammoma bodies might also be observed. In comparison, the micropapillary pattern has smaller papillae. It has no fibrovascular cores or blood vessels.

The associate editor coordinating the review of this manuscript and approving it for publication was Vishal Srivastava.

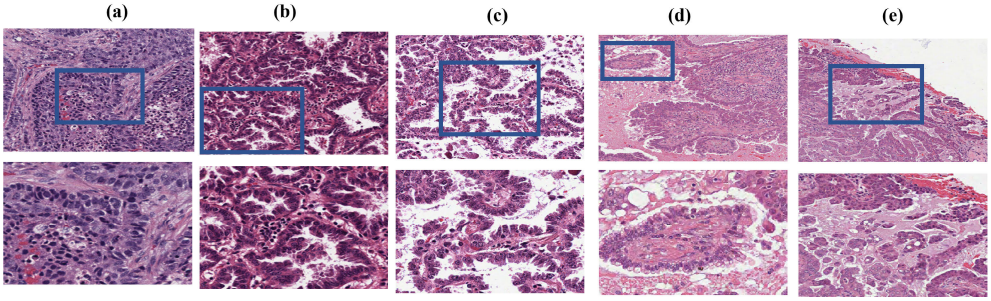

FIGURE 1. Sample images for LUAD tumour growth patterns. The first row shows a sample image for each pattern with close-up images on the bottom row: (a) solid, (b) acinar, (c) lepidic, (d) papillary and (e) micropapillary.

In 2011, the interdisciplinary research group of the International Association for the Study of Lung Cancer (IASLC), the American Thoracic Society (ATS) and the European Respiratory Society (ERS) published the revised LUAD classification system. The system recommends a semiquantitative estimation of each pattern in 5% increments [4]. This assessment has several advantages compared to the previous 10% increments: first, it allows greater flexibility in estimating the predominant pattern, especially when two patterns have similar percentages. Second, it reduces the risk of assigning 10% to small-size prognostically significant patterns, such as micropapillary. Third, it encourages pathologists to report all small-size patterns in the tumour. LUAD tumours are heterogeneous; most LUAD histology slides contain a mixture of growth patterns within one tumour section. The new classification system addresses this issue by introducing the term ''predominant pattern'' instead of the term ''mixed pattern'' that had been used since 2004 WHO lung classification [5]. A mixed pattern tumour has two or more patterns of different percentages. The term predominant pattern tumour, however, refers to the pattern with the largest percentage within a tumour. Other observed patterns should also be reported. Pathologists comprehensively assess all histology patterns they observe in the tumour. Then, they report all the patterns using 5% increments. Finally, they classify the tumour according to the predominant pattern [4]. In this study, a machine learning method was proposed for the automatic recognition of growth patterns and survival prediction. To the best of our knowledge, no work has been done to automatically classify the five growth patterns in LUAD for survival analysis. The proposed method mimics the visual inspection by the pathologist under the microscope at different magnification levels to recognise the growth patterns. The proposed method identified all five growth patterns by examining the tissue at several magnification levels. Tiles at several magnification levels were used to train the deep learning model and to examine the significance of the cellular and morphological features for identifying growth patterns.

II. RELATED WORK

Several studies have established the potential correlation between histology growth patterns and disease outcomes, such as overall survival (OS), disease-free survival (DFS) and response to chemotherapy. The micropapillary-predominant tumour is commonly associated with poor outcomes. Zhang et al. [6] and Russel et al. found that it has significantly poor survival. Cases with micropapillary pattern of at least 5% had worse DFS and were correlated with lymph node metastasis [7], [8] and poorly differentiated tumours [9]. Others reported that solid had an unfavourable prognosis with low DFS [1], [10], [11], [12]. Solid and micropapillary were reported to benefit from chemotherapy [11]. There is a significant agreement in the literature that lepidic-predominant pattern had a good prognosis and could benefit from chemotherapy [1], [10], [13], [14], [15]. It has also been shown that lepidic pattern is linked to the biological shift from in-situ to invasive LUAD [16]. Some studies had reported that acinar pattern had an intermediate-to-good prognosis [1], while others had shown that it is correlated with relatively poor prognosis [17] but may not benefit from chemotherapy treatment [11].

One reason behind the divergence in results above is the inter-and intra-observer variability due to the complex heterogeneity of LUAD tumours, the broad definition of histology growth patterns and the different forms and shapes these patterns could grow into. Erick et al. [18] investigated the issue of reproducibility in the histology growth pattern of pulmonary adenocarcinoma. They analysed the agreement between pathologist observations in typical and challenging cases for representative tumours and normal tissue samples. They reported the kappa score values of 0.77 ± 0.07 and 0.38 ± 0.14 for typical and challenging cases, respectively. For normal cases, however, the kappa score for typical and difficult cases dropped to 0.55 ± 0.06 and 0.08 ± 0.02, respectively. Acinar [19], papillary and micropapillary patterns [20] were found to be the most challenging patterns for the pathologists.

There are several approaches for automatically analysing LUAD whole slide images. Graham et al. [21] combined convolution neural network (CNN) classification and statistical and morphological analysis to classify image tiles into lung adenocarcinoma or lung squamous cell carcinoma. Alsubaie et al. [22] automatically classified tumour cells in LUAD WSI. They found that global nuclear morphometric features characterised by heatmap statistics significantly

correlated with LUAD overall survival. Gertych et al. [23] applied CNN and soft-voting to classify the four growth patterns of LUAD (solid, micropapillary, acinar, and cribriform). The correlation between the predominant pattern and disease outcome was not analysed. Xiao et al. [24] proposed to combine GNN and CNN modules to predict the LUAD growth patterns. The Graph convolutional networks (GCN) model was trained using the nuclear features, while the CNN model was trained using the whole image. Their approach requires huge computational resources for nuclei detection and segmentation. Furthermore, there might be feature redundancy in the GNN and CNN models. Wei et al. [25] applied the classical ResNet [26] to classify LUAD into the five growth pattern subtypes. Predominant patterns were estimated using a heuristic approach. The dataset was collected from a local institution, and the survival data were not provided.

III. DATASET AND METHODS

This study has two datasets collected from two different sources. The first dataset contained 10 H&E LUAD WSIs and was released by the CPM challenge during MICCAI 2017 [27]. The images were obtained from The Cancer Genome Atlas (TCGA) repository [28]. WSIs were reviewed by the pathologist and were made available in the Aperio SVS format. The original TCGA filename, the image label and metadata were removed from the image files. The complete discussion of this dataset and the CPM-MICCAI207 challenge can be found in Vu et al. [29]. The clinical information and patient survival for this dataset were not available. Therefore, this dataset was utilised to optimise the deep learning model and was not used for the survival analysis.

The second dataset was collected anonymously from the University Hospitals Coventry and Warwickshire (UHCW) NHS Trust in Coventry, UK. Informed consent was obtained from all participants, and clinical information was anonymously collected from clinical records and pathology reports. This study has approval from the National Research Ethics Service North West (REC reference 15/NW/0843). The entire study was performed in accordance with relevant guidelines and regulations.

This dataset consisted of 78 LUAD H&E WSI and was collected between 2006 and 2014. H&E slides were digitally scanned with a resolution of 0.275μm/pixel using VL120 Scanner (Omnyx LLC). The pulmonary pathologist (DS) reviewed all the slides and excluded 14 slides which were not suitable for the study (e.g., not LUAD, out-of-focus slides, lot of artefacts, etc.). Table 1 shows a summary of the patient clinical information in our cohort. The average age is 68, and 52% of the patients were in the early stage of LUAD. Vascular invasion was detected in 50% of the cases, and the overall survival is 51 months on average. From 2006 to 20014, 47% of the patients in this cohort died.

The study has two parts: in the first part, the classification performance of the proposed model was examined at multiple magnification levels. The magnification level which achieves the best performance was selected to train the deep learning model. In the second part, the chosen deep learning model was used to classify the WSIs. Percentages of each GP were automatically calculated to perform the survival analysis. In this paper, we extend our initial findings in [31] by applying the classification model to another dataset and analysing the correlation between the percentage of LUAD growth pattern and overall survival.

TABLE 1. Summary of clinicopathologic features of the UHCW cohort.

Clinical characteristics of the LUAD cohort	
Number of patients	78
Age (years)	68
Survival (months)	51
Number of patients who died	34 (44%)
LUAD stage	
Stage I	41 (53%)
Stage II	20 (26%)
Stage III	14 (18%)
Info is unavailable	3 (4%)
Grade of tumour differentiation	
Grade 1	11 (14%)
Grade 2	27 (35%)
Grade 3	25 (32%)
Info is unavailable	15 (19%)
Vascular invasion	
Vascular invasion is detected	39 (50%)
Vascular invasion is not undetected	37 (47%)
Info is unavailable	4 (5%)

The pipeline of our study is shown in Figure 3. Initially, training the deep learning model to classify each tile of the WSI into one of the six classes: acinar, papillary, micropapillary, solid, lepidic and ''others''; ''others'' are all the non-pattern image tiles including the following:

- Background: total or partial glass and appears as a white region in the WSI;
- Non-tumour tissue: e.g., stromal tissue, smooth muscles and necrosis;
- A group of scattered tumour cells that do not form any pattern or structural formation.

Figure 2 shows examples of the class ''others''. Two pathologists, DS and AK, annotated 10 WSIs of H&E LUAD using the Automated Slide Analysis Platform (ASAP). We generated tiles (training images) using the annotated regions. Tile is extracted at four different magnification levels, such that the context surrounding the centre point is gradually increased from the highest magnification to the lowest. The maximum context is captured at the lowest magnification. Therefore, there are four training sets (40×, 20×, 10× and 5×). In each set, we had six classes: solid, acinar, papillary, lepidic, micropapillary and others. Figure 4 shows example images for each dataset.

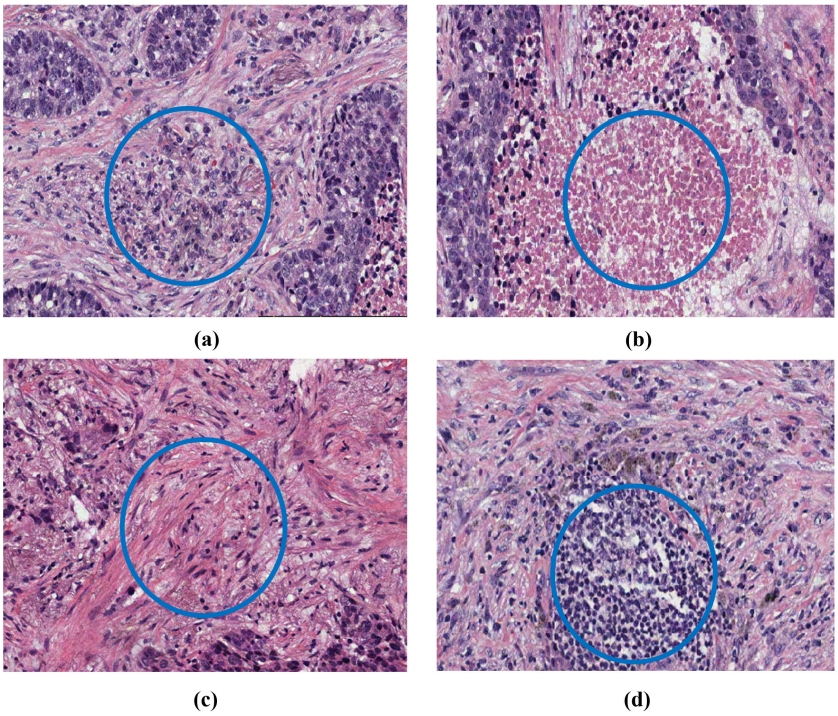

FIGURE 2. Examples of non-growth pattern tumour tissue. Tissues shown in these images are all labelled as "others". (a) Distinct tumour cells which do not form any specific pattern. (b) Necrosis cells are caused by dead cells. (c) Stromal cells and (d) inflammatory cells.

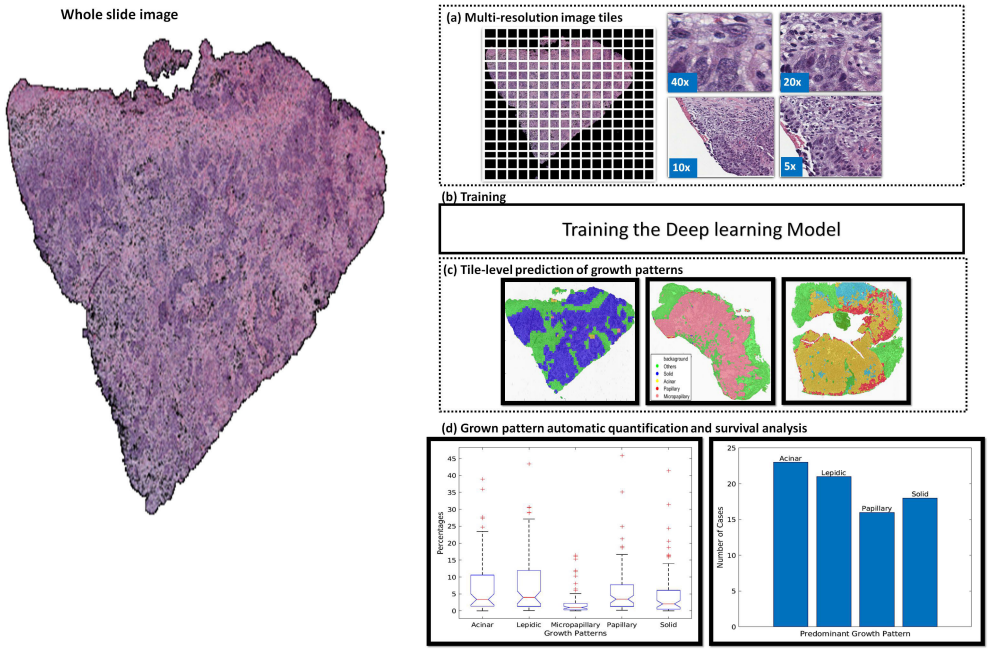

FIGURE 3. Framework for the automatic classification of GP and the LUAD survival analysis. (A) shows the steps for preparing the training set and building the classification model. (C) shows the GP classification per WIS from the CPM-MICCAI2017. The figure is generated using MATLAB R2018b [30](D) The final step is the statistical and survival analysis.

A. GROWTH PATTERN CLASSIFICATION IN THE WHOLE SLIDE IMAGE

Table 2 shows the tile classification accuracy and the mean accuracy per magnification level. Implementation details are given in the Result section in the Supplementary Materials. The model was trained on 40× and had the lowest mean accuracy of 86%, while the highest accuracy (93%) was achieved when training on 5× magnification. Training on images of

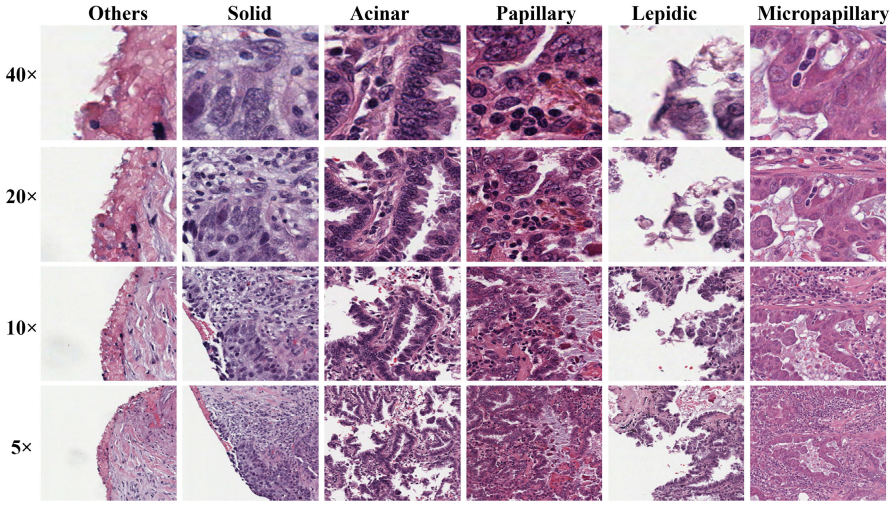

FIGURE 4. Sample training images from the CPM-MICCAI2017 dataset. Each row represents one magnification level. Each column represents images for the same class extracted in a decreasing resolution. The context gradually increases when increasing the magnification level while maintaining the same image size. In the 40× dataset, cellular information is noticeable; As the magnification decreases, cells show some structural arrangements.

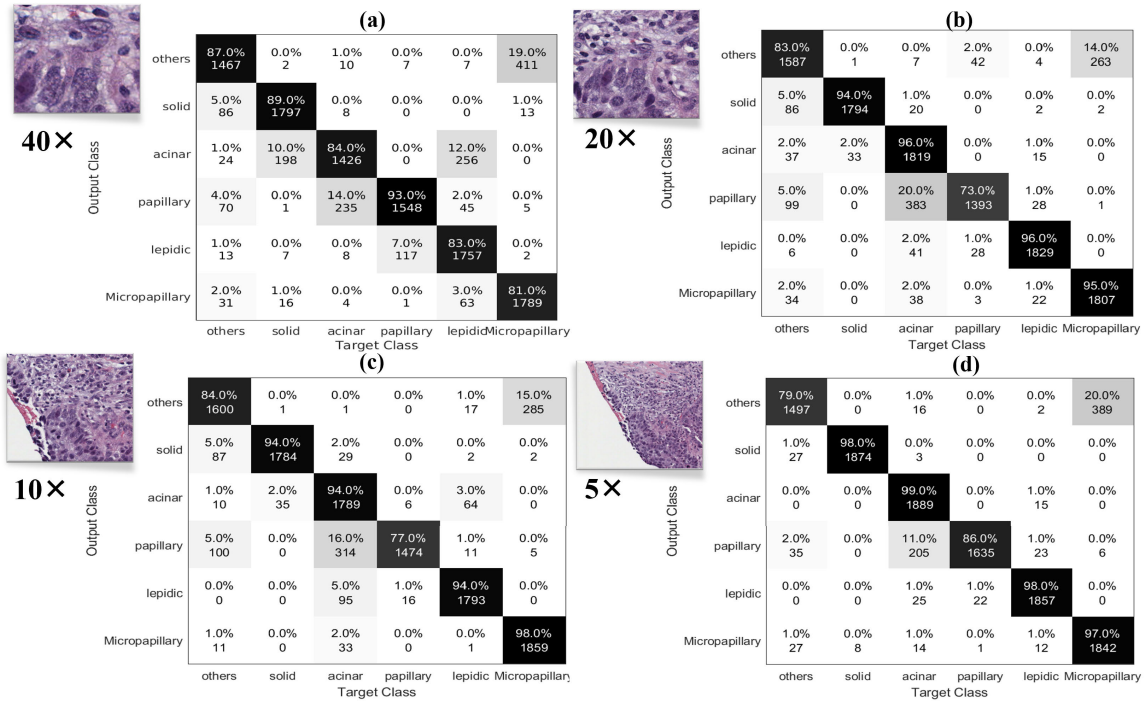

FIGURE 5. Confusion matrices for ResNet50 trained using CPM-MICCAI2017 dataset on four different magnifications (40×, 20×, 10× and 5× magnifications). A sample training image is shown in the top left corner of each confusion matrix.

20× and 10× magnifications improved the mean performance compared to 40×. The reason for accuracy degradation using 40× might be the lack of structural morphology of the tumour tissue, which is critical in distinguishing between the growth patterns. Therefore, there is uncertainty in class prediction especially patterns with similar morphology (e.g., papillary and acinar, acinar and lepidic); see Figure 5 (a). On the other hand, context captured by 5× magnification achieved the best performance on tile-level classification. The increase in perdition accuracy is due to the ability of the deep learning model to learn the spatial distribution of nuclei, the overall tissue morphology and the surrounding context of the pattern. However, the wider context may cause misclassification, such as the results obtained from the other and micropapillary classes (see Figure 5 (d). Detailed performance for the 20× and 10× are shown in Figure 5 (b,c).

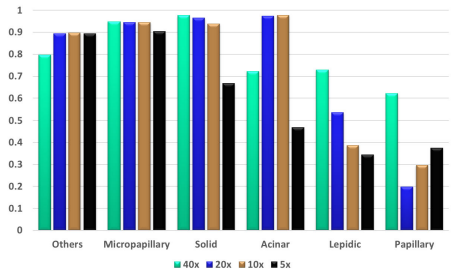

FIGURE 6. Dice measure for the overall slide pattern classification accuracy. The y-axis represents the Dice accuracy in [0,1], and the x-axis shows pattern labels.

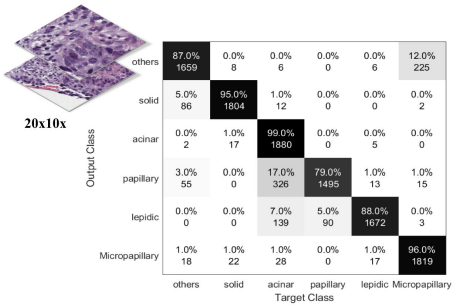

FIGURE 7. Confusion matrix for the proposed training model. The model had difficulty identifying lepidic from acinar and papillary patterns, reducing overall accuracy.

TABLE 2. Accuracy on validation set for ResNet50 trained using the CPM-MICCAI2017 dataset on four different magnifications (40×, 20×, 10× and 5×). For each magnification level, the best and worst accuracy per pattern were highlighted in bold and italic, respectively.

Magnification	Solid	Acinar	Papillary	Lepidic	Micropapillary	Others	Mean
40×	89%	84%	**93%**	83%	*81%*	87%	86%
20×	94%	**96%**	*73%*	**96%**	95%	83%	90%
10×	94%	94%	*77%*	94%	**98%**	84%	90%
5×	98%	**99%**	86%	98%	97%	*79%*	93%

TABLE 3. Validation accuracy for ResNet50 trained using the CPM-MICCAI2017 dataset on 20×, 10× and the two magnifications combined (20× & 10×). For each magnification, the best and the worst accuracy are highlighted in bold and italic, respectively.

Magnification	Solid	Acinar	Papillary	Lpidic	Micropapillary	Others	Mean
20×	94%	**96%**	73%	**96%**	95%	83%	90%
10×	94%	94%	77%	94%	**98%**	84%	90%
20× & 10 ×	95%	**99%**	79%	88%	96%	87%	**91%**

Next, we performed a tile-level growth pattern classification on the test set of three WSI. The class label with maximum probability (from all six classes) was used to assign the final classification per tile. The average Dice coefficient per magnification level is shown in Figure 6. We found that 5× performed worse for most of the patterns on WSI tile-based classification due to the reasons discussed above. We found that 20× and 10× performed better in the validation and testing sets. In summary, tiles at 5× and 40× were excluded, and tiles at 20× and 10× were selected. We retrained the deep learning model using stacked images from 20× and 10× magnifications. Therefore, we have 224 × 24 × 6 training images. We found that by providing more contextual information, the overall performance was increased as shown in Table 3. Moreover, the classification accuracy for acinar, papillary and the class others were significantly improved. Solid and micropapillary achieved similar performance compared to the individual 20× and 10× models. Table 3 shows a significant decrease in the lepidic pattern; the reason could be the additional context captured by the 10× tile. Hence, the classification of the patterns lepidic, micropapillary and papillary is affected by the fact that the three patterns share some architectural features, such as the white background and fibrovascular cores. The corresponding confusion matrix is shown in Figure 7.

The final step is the WSI classification. We applied the same tile classification approach mentioned above using the 20×, 10× trained model. Sample WSI tile-based classification results are shown in Figure 8. The tumour has a predominant acinar pattern with few instances of lepidic and micropapillary patterns. One sample region for each class is shown with the corresponding box colour on the right. It is common to have lepidic and micropapillary patterns growing into each other. Therefore, some misclassification of these two patterns is expected. However, there are several ways to overcome this issue. First, annotation plays a vital role in the accuracy of the deep learning model. Given the subjectivity that comes with human assessment, it is essential to have consistent, good-quality annotations where patterns are relatively separated with minimum overlap. Second, all possible variations of each pattern must be included in the training dataset. LUAD tumour is heterogeneous; an individual pattern may grow into several morphological structures. One example is the solid pattern that could appear as scattered nests of tumour cells or one sheet of malignant cells with no gland formation. Another example is the acinar pattern, where glands grow in different sizes and shapes for varying levels of tumour differentiation, see Figure 9. Therefore, it is crucial to include all possible variations of each pattern in the training dataset. Otherwise fine-tuning might be an alternative solution [32], [33], [34]. More pattern classification results are shown in the Supplementary Materials.

B. QUANTIFICATION OF GROWTH PATTERNS AND CORRELATION WITH LUAD OVERALL SURVIVAL

The second dataset collected from the UHCW was used to perform the survival analysis. Pathologists DS and AK annotated samples for each pattern in 19 WSIs. Pathologists annotated regions of interest and assigned labels according to the six tissue types: solid, acinar, papillary, lepidic, micropapillary and others. Training images were generated by dividing the WSI into 224 × 224 grid. The centre point of each square was used as a reference point to extract two consecutive image tiles at 20× & 10× magnifications. Tissue artefacts and stain variability were considered by applying stain normalisation [35] and data augmentations such as flipping, rotation, adding noise and altering colour contrast. We used 80% tiles per class for training and 20% per class for validation; this

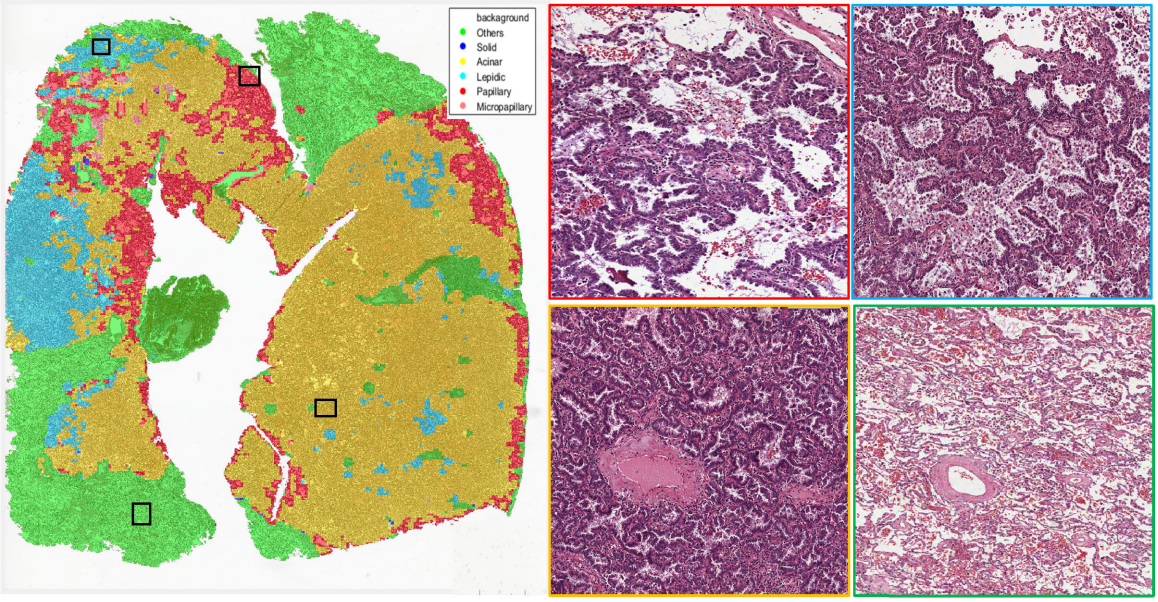

FIGURE 8. Sample WSI tile-based classification result on the CPM-MICCAI2017 dataset. The image in the first column (left) shows the classification results for a mixed pattern WSI. The deep learning model is trained on a combination of image tiles at 20× & 10× magnifications. Small boxes on the left image are shown with higher magnification on the right. The colour of each box corresponds to the tissue type. The figure is generated using MATLAB R2018b [30].

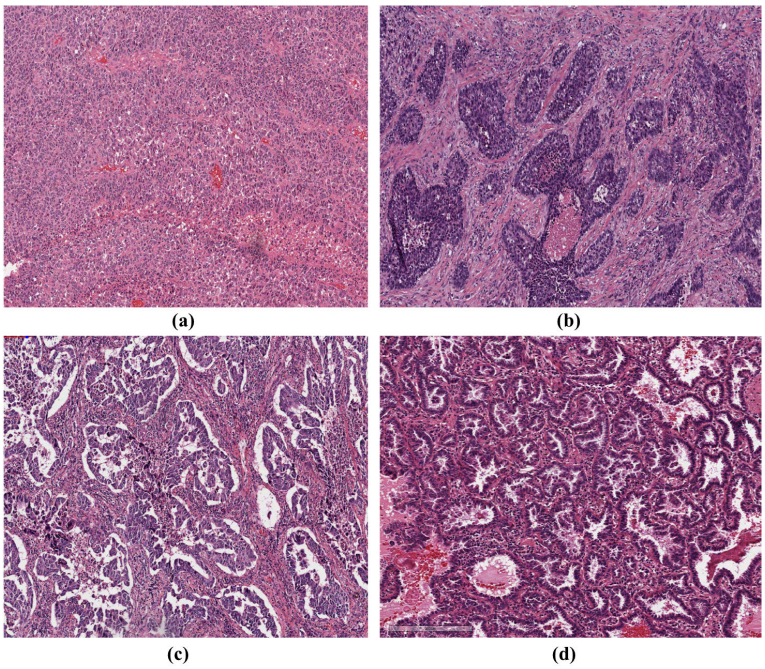

FIGURE 9. Sample images for solid (a,b) and acinar (c,d) patterns from the CPMMICCAI2017 dataset. The solid pattern varies across different tissues. Glandular formation in the acinar pattern also has a variable appearance in the low (c) and high (d) grade tumours.

gave 9,168 and 2,292 image tiles per class for training and testing, respectively. Table 4 shows tile-level classification accuracy for the UHCW dataset.

The whole slide image was classified at 10× to speed up the processing time. Each WSI was divided into small tiles of size 224 × 224. Tiles were extracted at 20× & 10× concatenated on the third dimension. Each case in the UHCW cohort had five probability maps, each corresponding to one class. We found the class of the tile by taking the maximum probability of the five patterns. Figure 10 shows WSI tile-based classification results.

C. AUTOMATIC QUANTIFICATION OF GROWTH PATTERNS IN WSIs

The growth pattern was quantified by counting the number of tiles per pattern; which was then divided by the number of

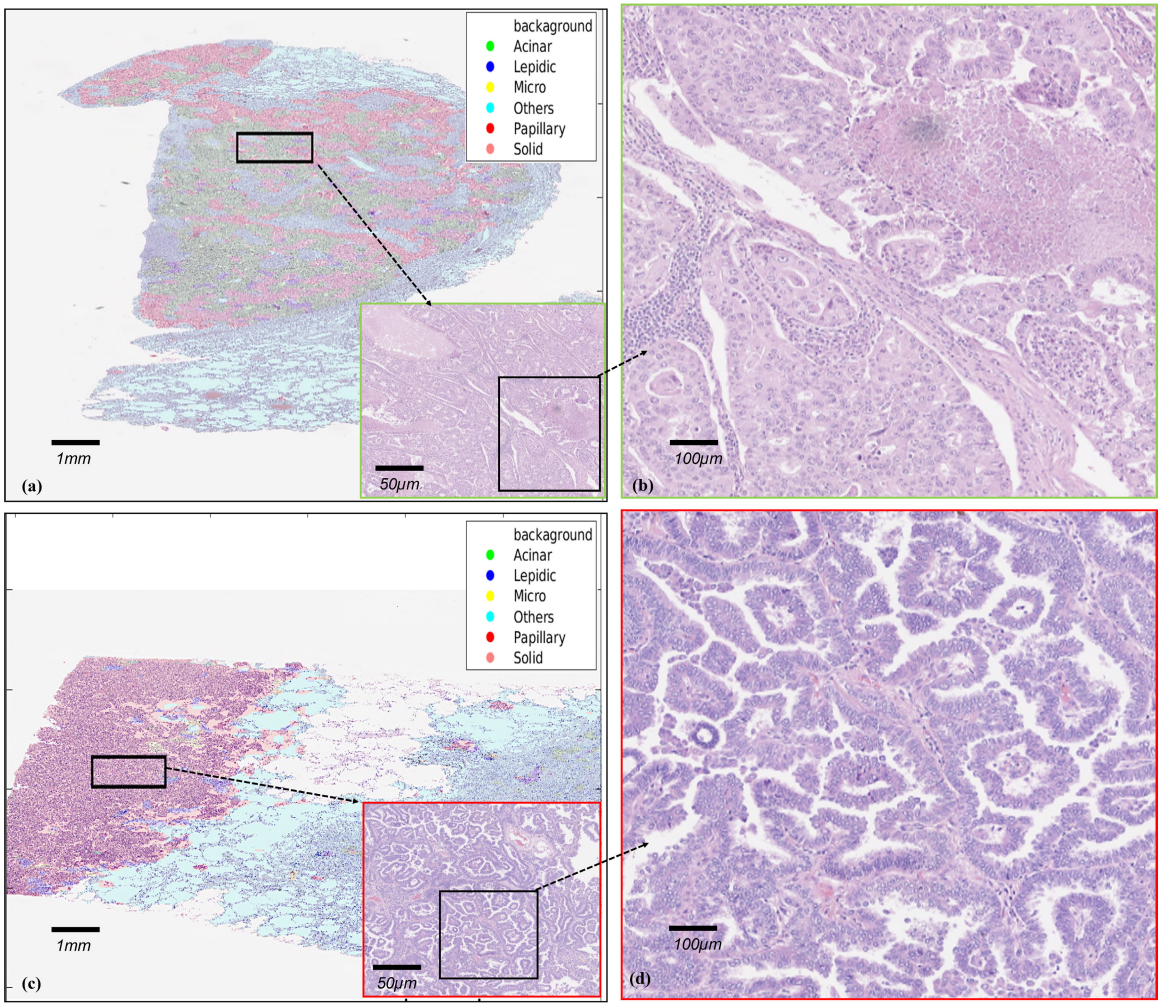

FIGURE 10. Tile-base classification for automatic pattern quantification using the UHCW dataset. (a) WSI of the acinar-predominant pattern. The largest percentage is for acinar, followed by papillary and then solid. The region inside the box is shown in (b). (c) WSI of the papillary-predominant pattern. The papillary pattern dominates this tumour section, while the remaining tissue constitutes either non-tumour or stromal tissue. Areas of the papillary pattern are shown in (d).

TABLE 4. Tile-level accuracy for ResNet50 trained using UHCW dataset. The highest accuracy per pattern is shown in bold.

Magnification	Solid	Acinar	Papillary	Lepidic	Micropapillary	Others	Mean
40×	89%	88%	89%	85%	88%	86%	87%
20×	96%	89%	93%	94%	97%	94%	93%
10×	**99%**	95%	**98%**	94%	98%	97%	96%
20× &10×	98%	**96%**	**98%**	**95%**	**99%**	**98%**	**97%**

non-empty tiles in the WSI. Figure 11 (a) shows a box plot of pattern percentages in the whole dataset. The micropapillary pattern had the lowest percentage in our cohort. Although micropapillary normally occurs in small percentages [15], [36], a large number of cases of the micropapillary pattern is necessary to analyse the impact on patient survival. The acinar pattern was the most common in our dataset, i.e., most cases had a percentage of acinar. The plot shows that the median acinar percentage was 3% of the tissue size. The second most frequent pattern was lepidic, with a median percentage of 4%. Then, papillary with a median of 3%, solid with a median of 2% and lastly, micropapillary with a median of approximately 1%. Next is the analysis of the overall patient survival and the five-year survival.

Figure 11 (b) shows the number of cases for each predominant pattern. Micropapillary-predominant pattern was not encountered in our dataset. Acinar is one of the most common predominant patterns in LUAD and usually has a good prognosis. Therefore, cases with acinar-predominant pattern have longer survival and follow-up periods. This observation applies to our cohort; 23 (29%) cases had the acinar-predominant pattern. There were 21 cases (27%) with the lepidic-predominant pattern, 16 cases (21%) with the papillary-predominant pattern, 18 (23%) cases had the solid-predominant pattern and 10 cases (10%) had at least 1% of the micropapillary pattern.

D. SURVIVAL ANALYSIS USING AUTOMATIC QUANTIFICATION OF PREDOMINANT PATTERN

This section investigated the impact of the predominant pattern on LUAD patient survival. In Figure 12, the

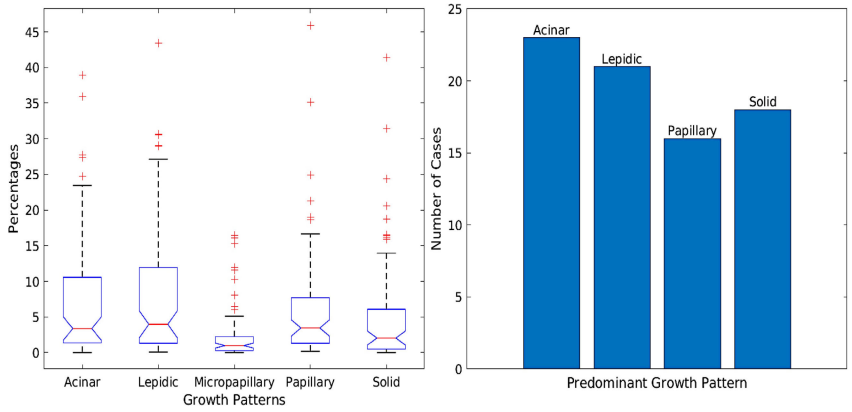

FIGURE 11. Growth pattern quantification using the UHCW cohort. (a) Pattern percentages for all cases. (b) The number of cases per predominant pattern.

TABLE 5. Multivariate analysis of the prognostic significance of growth pattern. The predictive power of each feature was measured by fitting a logistic regression model according to patient five-year survival. Significant *p*- values are shown in bold. β: correlation coefficient, CI: confidence interval.

Growth Pattern	β	HR (95% CI for HR)	p-value
Acinar	0.042	-0.041 0.123	0.301
Lepidic	0.196	0.080 0.367	0.0058
Papillary	0.067	-0.035 0.181	0.188
Solid	0.005	-0.159 0.150	0.945
Micropapillary	-0.465	-0.967 -0.113	0.032

TABLE 6. Multivariate analysis of the prognostic significance of growth pattern. Significant *p*-values are shown in bold. β: correlation coefficient, HR: hazard ratio, CI: confidence interval.

Growth Pattern	β	HR (95% CI for HR)	p-value
Age	0.3726	1.452 (0.668-3.154)	0.347
Vascular-invasion	1.063	2.896 (1.245-6.736)	0.0135
Tumour site	-0.105	0.8999 (0.415-1.953)	0.790
Tumour stage	-0.125	0.882 (0.566-1.376)	0.581
Model score	-1.090	0.336 (0.135-0.835)	0.019

Kaplan-Meier plots show the overall survival probability in the UHCW dataset for each predominant pattern. It shows that patients with the lepidic-predominant and acinar-predominant patterns had the highest survival, compared to the other predominant patterns, especially in the first five years (60 months). On the other hand, patients with the papillary-predominant and solid-predominant patterns had the lowest survival probability. Our dataset did not have cases with the micropapillary-predominant pattern. Therefore, we could not investigate the correlation between patient survival and micropapillary-predominant pattern. Other clinical factors such as age and vascular invasion affect the overall survival, which could be one of the reasons the lepidic curve fell after 60 months. Next, we looked at each pattern individually and compared the overall survival for each predominant pattern against all other patterns. Figure 12 (b) shows that cases with a papillary-predominant pattern are more likely to have lower survival than non-papillary cases. Figure 12 (d) shows that patients with lepidic-predominant pattern had higher survival probability than cases with other predominant patterns, especially in the first five years (60 months).

Next, we investigated the impact of the combined five growth patterns (the five growth pattern fingerprinting) on LUAD five-year survival. We employed a logistic regression using the UHCW dataset. The five-year survival was considered as a binary variable, such that patients with greater than five-year survival had a value of 1; 0 otherwise. We split data into 60% for training and 40% for testing. Per case, the percentage of each growth pattern was computed and collected into one feature vector. We fit a logistic regression model using the **glm** function in **R**. The model had an accuracy of 0.826 on the training set and an area under the curve of 0.65 for the testing set. The predictive power and the *p*-value for each growth pattern are shown in Table 5. The correlation between the model scoring and the overall survival is also shown in Figure 12 (f). The plot shows that the model split our cohort into good and bad overall prognosis. Hence, patients with a higher probability of survival for more than five years have longer overall survival and vice versa. A multivariate analysis using growth-pattern-based model prediction is shown in Table 6. The model is also significant as an independent predictor based on the univariate analysis with $p = 0.013$ and a correlation coefficient of -1.0713, with a confidence interval [0.147, 0.799].

IV. DISCUSSION

This work presents an automated growth pattern recognition and classification for LUAD whole slide images, the most common non-small cell lung carcinomas. Manual size estimation of growth patterns can be replaced by AI-based methods, which can be used as a second opinion system. The key observations from this work are as follows:

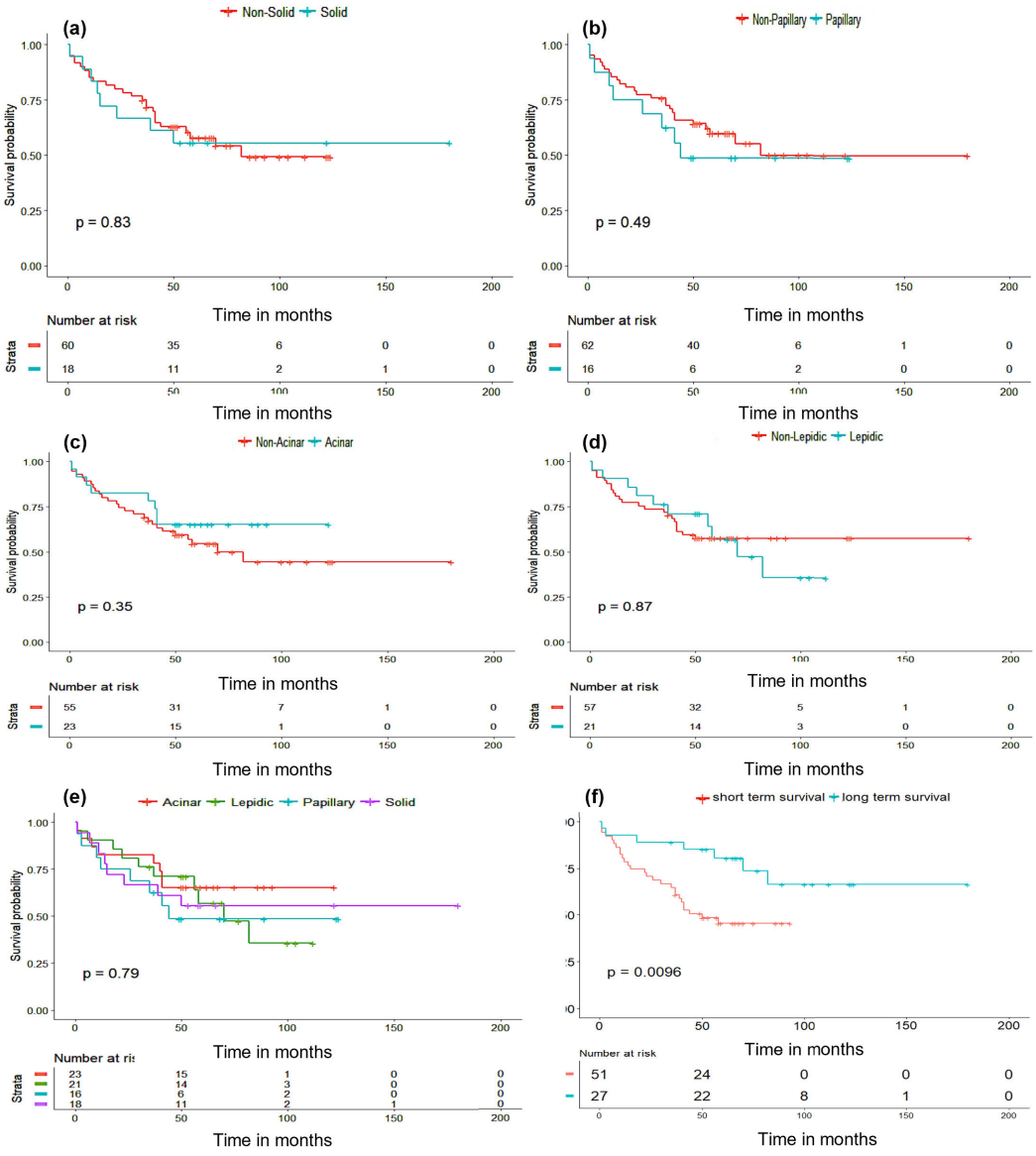

FIGURE 12. (a,b,c and d) are the Kaplan-Meier overall survival plots for each pattern independently against all other patterns in the UHCW cohort. (e) Kaplan-Meier overall survival plot for all patterns against each other. (f) Kaplan-Meier plot using model prediction based on WSI percentages of growth patterns. The model prediction is correlated with overall patient survival.

- The use of a machine learning-based method to tackle growth pattern quantification could provide an objective and reproducible estimation.
- LUAD is a complicated tumour where multiple patterns may intersect within the same tumour. However, it is crucial to estimate each pattern's percentage as it correlates with patient survival and disease outcome.
- The deep learning model shows high performance in locating and classifying the five growth patterns in LUAD whole slide images.
- Finding of this study correlates with the clinical observation regarding patient survival. We find that patients with lepidic-predominant and acinar-predominant have a higher probability of five-year survival than other predominant patterns. Therefore, accurate percentage estimation is necessary to analyse the correlation with patient survival, hence, the treatment plan.
- Micropapillary pattern normally had worse survival. However, it grows in small percentages compared to other patterns in the same slide. Therefore, no micropapillary predominant cases were encountered in this dataset. However, having at least 1% of the micropapillary pattern were correlated with five-year survival p-value$<$0.032, 5
- This study opens new doors by providing a baseline to explore the growth pattern classification in histopathology images and investigates its impact on disease outcome. However, its limitation is the size of the dataset used. In the future, the dataset size should be increased.

V. STUDY LIMITATIONS

Based on the specification of our dataset and the results from our analysis, we hypothesised that quantified percentages of the LUAD growth patterns are potential predictors of LUAD five-year survival. However, our study has the limitation that our survival analysis was based on a single dataset collected from one medical centre. Therefore, the dataset is relatively small, and some patterns were rare in our cohort (e.g. micropapillary). Therefore, we were limited in our experimental setting. Collecting large-scale data from multiple centres with complete histological and clinical information is required.

VI. SUMMARY

This paper proposed a multi-resolution deep learning model to automatically classify WSIs of LUAD into the five histology growth patterns. We trained our model using a gradually increased context from one magnification level to the next. We found that the model requires cellular information and morphological architecture to differentiate between the growth patterns. We trained the ResNet deep learning model on image tiles extracted from two magnification levels and found that the overall accuracy was increased. We analysed the impact of the predominant growth pattern on LUAD overall survival. Tile-based classification of growth pattern is performed to find the predominant pattern per WSI automatically. We then built a five-year survival classification model using percentages of growth patterns. The lepidic and micropapillary patterns had a strong correlation with LUAD five-year survival. The model successfully classified our cohort into good and bad prognosis.

ACKNOWLEDGMENT

This research was funded by Princess Nourah bint Abdulrahman University Researchers Supporting Project number (PNURSP2023R321), Princess Nourah bint Abdulrahman University, Riyadh, Saudi Arabia. The authors would like to thank Professor Ali Khurram from The University of Sheffield for reviewing the annotated slides.

REFERENCES

[1] P. A. Russell, Z. Wainer, G. M. Wright, M. Daniels, M. Conron, and R. A. Williams, "Does lung adenocarcinoma subtype predict patient survival?: A clinicopathologic study based on the new international association for the study of lung cancer/American thoracic society/European respiratory society international multidisciplinary lung adeno," *J. Thoracic Oncol.*, vol. 6, pp. 1496–1504, Sep. 2011.

[2] P. A. Russell and G. M. Wright, "Predominant histologic subtype in lung adenocarcinoma predicts benefit from adjuvant chemotherapy in completely resected patients: Discovery of a holy grail?" *Ann. Transl. Med.*, vol. 4, no. 1, p. 16, Jan. 2016.

[3] W. D. Travis, E. Brambilla, A. G. Nicholson, Y. Yatabe, J. H. M. Austin, and M. B. Beasley, "The 2015 world health organization classification of lung tumors: Impact of genetic, clinical and radiologic advances since the 2004 classification," *J. Thoracic Oncol.*, vol. 10, no. 9, pp. 1243–1260, 2015.

[4] W. D. Travis, E. Brambilla, and M. Noguchi, "International association for the study of lung cancer/American thoracic society/European respiratory society international multidisciplinary classification of lung adenocarcinoma," *J. Thoracic Oncol.*, vol. 6, no. 2, pp. 244–285, Feb. 2011.

[5] M. B. Beasley, E. Brambilla, and W. D. Travis, "The 2004 world health organization classification of lung tumors," *Seminars Roentgenology*, vol. 40, no. 2, pp. 90–97, Apr. 2005.

[6] Y. Zhang, R. Wang, D. Cai, Y. Li, Y. Pan, H. Hu, L. Wang, H. Li, T. Ye, X. Luo, Y. Zhang, B. Li, L. Shen, Y. Sun, and H. Chen, "A comprehensive investigation of molecular features and prognosis of lung adenocarcinoma with micropapillary component," *J. Thoracic Oncol.*, vol. 9, no. 12, pp. 1772–1778, Dec. 2014.

[7] M. S. Roh, J. I. Lee, P. J. Choi, and Y. S. Hong, "Relationship between micropapillary component and micrometastasis in the regional lymph nodes of patients with stage i lung adenocarcinoma," *Histopathology*, vol. 45, no. 6, pp. 580–586, Dec. 2004.

[8] T. Kawakami, K. Nabeshima, M. Hamasaki, A. Iwasaki, T. Shirakusa, and H. Iwasaki, "Small cluster invasion: A possible link between micropapillary pattern and lymph node metastasis in pT1 lung adenocarcinomas," *Virchows Archiv*, vol. 454, no. 1, pp. 61–70, Jan. 2009.

[9] J. Zugazagoitia, A. B. Enguita, J. A. Nuñez, L. Iglesias, and S. Ponce, "The new IASLC/ATS/ERS lung adenocarcinoma classification from a clinical perspective: Current concepts and future prospects," *J. Thoracic Disease*, vol. 6, no. 5, pp. S526–S536, 2014.

[10] L. M. Solis, C. Behrens, M. G. Raso, H. Y. Lin, H. Kadara, P. Yuan, H. Galindo, X. Tang, J. J. Lee, N. Kalhor, I. I. Wistuba, and C. A. Moran, "Histologic patterns and molecular characteristics of lung adenocarcinoma associated with clinical outcome," *Cancer*, vol. 118, no. 11, pp. 2889–2899, Jun. 2012.

[11] M.-S. Tsao, S. Marguet, G. Le Teuff, S. Lantuejoul, F. A. Shepherd, L. Seymour, R. Kratzke, S. L. Graziano, H. H. Popper, R. Rosell, J.-Y. Douillard, T. Le-Chevalier, J.-P. Pignon, J.-C. Soria, and E. M. Brambilla, "Subtype classification of lung adenocarcinoma predicts benefit from adjuvant chemotherapy in patients undergoing complete resection," *J. Clin. Oncol.*, vol. 33, no. 30, pp. 3439–3446, Oct. 2015.

[12] M. Riquet and C. Foucault, "Prognostic value of histology in resected lung cancer with emphasis on the relevance of the adenocarcinoma subtyping," *Ann. Thoracic Surg.*, vol. 81, pp. 1988–1995, Jun. 2006.

[13] S. Sasada, Y. Miyata, T. Mimae, T. Mimura, and M. Okada, "Impact of lepidic component occupancy on effects of adjuvant chemotherapy for lung adenocarcinoma," *Ann. Thoracic Surgery*, vol. 100, no. 6, pp. 2079–2086, Dec. 2015.

[14] Y. Moon, S. W. Sung, K. Y. Lee, Y. K. Kim, and J. K. Park, "The importance of the lepidic component as a prognostic factor in stage I pulmonary adenocarcinoma," *World J. Surgical Oncol.*, vol. 14, no. 1, p. 37, Dec. 2016.

[15] J. H. von der Thüsen, Y. S. Tham, H. Pattenden, A. Rice, M. Dusmet, E. Lim, and A. G. Nicholson, "Prognostic significance of predominant histologic pattern and nuclear grade in resected adenocarcinoma of the lung: Potential parameters for a grading system," *J. Thoracic Oncol.*, vol. 8, no. 1, pp. 37–44, Jan. 2013.

[16] D. A. Moore, M. Sereno, M. Das, J. D. Baena Acevedo, S. Sinnadurai, C. Smith, A. McSweeney, X. Su, L. Officer, C. Jones, K. Dudek, D. Guttery, P. Taniere, R. V. Spriggs, and J. Le Quesne, "In situ growth in early lung adenocarcinoma may represent precursor growth or invasive clone outgrowth—A clinically relevant distinction," *Modern Pathol.*, vol. 32, no. 8, pp. 1095–1105, Aug. 2019.

[17] G. Lin, H. Li, J. Kuang, K. Tang, Y. Guo, A. Han, and C. Xie, "Acinar-predominant pattern correlates with poorer prognosis in invasive mucinous adenocarcinoma of the lung," *Amer. J. Clin. Pathol.*, vol. 149, no. 5, pp. 373–378, Mar. 2018.

[18] E. Thunnissen et al., "Reproducibility of histopathological subtypes and invasion in pulmonary adenocarcinoma. An international interobserver study," *Modern Pathol.*, vol. 25, no. 12, pp. 1574–1583, Dec. 2012.

[19] Y.-C. Yeh, J.-I. Nitadori, K. Kadota, A. Yoshizawa, N. Rekhtman, A. L. Moreira, C. S. Sima, V. W. Rusch, and P. S. Adusumilli, "Using frozen section to identify histological patterns in stage I lung adenocarcinoma of ≤3cm: Accuracy and interobserver agreement," *Histopathology*, vol. 66, no. 7, pp. 922–938, May 2015.

[20] A. Warth, A. Stenzinger, A.-C. von Brünneck, B. Goeppert, J. Cortis, I. Petersen, H. Hoffmann, P. A. Schnabel, and W. Weichert, "Interobserver variability in the application of the novel IASLC/ATS/ERS classification for pulmonary adenocarcinomas," *Eur. Respiratory J.*, vol. 40, no. 5, pp. 1221–1227, Nov. 2012.

[21] S. Graham, M. Shaban, T. Qaiser, N. A. Koohbanani, S. A. Khurram, and N. Rajpoot, "Classification of lung cancer histology images using patch-level summary statistics," *Proc. SPIE*, vol. 10581, Mar. 2018, Art. no. 1058119.

[22] N. M. Alsubaie, D. Snead, and N. M. Rajpoot, "Tumour nuclear morphometrics predict survival in lung adenocarcinoma," *IEEE Access*, vol. 9, pp. 12322–12331, 2021.
[23] A. Gertych, Z. Swiderska-Chadaj, Z. Ma, N. Ing, T. Markiewicz, S. Cierniak, H. Salemi, S. Guzman, A. E. Walts, and B. S. Knudsen, "Convolutional neural networks can accurately distinguish four histologic growth patterns of lung adenocarcinoma in digital slides," *Sci. Rep.*, vol. 9, no. 1, pp. 1–12, Feb. 2019.
[24] W. Xiao, Y. Jiang, Z. Yao, X. Zhou, X. Sui, and Y. Zheng, "LAD-GCN: Automatic diagnostic framework for quantitative estimation of growth patterns during clinical evaluation of lung adenocarcinoma," *Frontiers Physiol.*, vol. 13, p. 1509, Aug. 2022.
[25] J. W. Wei, L. J. Tafe, Y. A. Linnik, L. J. Vaickus, N. Tomita, and S. Hassanpour, "Pathologist-level classification of histologic patterns on resected lung adenocarcinoma slides with deep neural networks," *Sci. Rep.*, vol. 9, no. 1, pp. 1–8, Mar. 2019.
[26] K. He, X. Zhang, S. Ren, and J. Sun, "Deep residual learning for image recognition," in *Proc. IEEE Conf. Comput. Vis. Pattern Recognit. (CVPR)*, Jun. 2016, pp. 770–778.
[27] "Computational precision medicine challenge," in *Proc. MICCAI*, QC, Canada, 2017.
[28] *The Cancer Genome Atlas Program*, Nat. Institutes Health, Bethesda, MD, USA, 2006.
[29] Q. D. Vu, S. Graham, T. Kurc, M. N. N. To, M. Shaban, T. Qaiser, N. A. Koohbanani, S. A. Khurram, J. Kalpathy-Cramer, T. Zhao, R. Gupta, J. T. Kwak, N. Rajpoot, J. Saltz, and K. Farahani, "Methods for segmentation and classification of digital microscopy tissue images," *Frontiers Bioeng. Biotechnol.*, vol. 7, p. 53, Apr. 2019.
[30] *(R2018a)*, MATLAB, MathWorks, Natick, MA, USA, 2018. Accessed: Feb. 2, 2022.
[31] N. Alsubaie, M. Shaban, D. Snead, A. Khurram, and N. Rajpoot, "A multi-resolution deep learning framework for lung adenocarcinoma growth pattern classification," in *Proc. Annu. Conf. Med. Image Understand. Anal.* Cham, Switzerland: Springer, 2018, pp. 3–11.
[32] H. Jung, S. Lee, J. Yim, S. Park, and J. Kim, "Joint fine-tuning in deep neural networks for facial expression recognition," in *Proc. IEEE Int. Conf. Comput. Vis. (ICCV)*, Dec. 2015, pp. 2983–2991.
[33] N. Becherer, J. Pecarina, S. Nykl, and K. Hopkinson, "Improving optimization of convolutional neural networks through parameter fine-tuning," *Neural Comput. Appl.*, vol. 31, pp. 3469–3479, Nov. 2017.
[34] G. Gando, T. Yamada, H. Sato, S. Oyama, and M. Kurihara, "Fine-tuning deep convolutional neural networks for distinguishing illustrations from photographs," *Exp. Sys. Appl.*, vol. 66, pp. 295–301, Dec. 2016.
[35] E. Reinhard, M. Adhikhmin, B. Gooch, and P. Shirley, "Color transfer between images," *IEEE Comput. Graph. Appl.*, vol. 21, no. 4, pp. 34–41, Jul. 2001.
[36] R. D. O. D. Achcar, M. N. Nikiforova, and S. A. Yousem, "Micropapillary lung adenocarcinoma," *Amer. J. Clin. Pathol.*, vol. 131, no. 5, pp. 694–700, May 2009.

NAJAH ALSUBAIE received the Ph.D. degree from the Department of Computer Science, The University of Warwick, Coventry, U.K., in January 2019. During her Ph.D. degree, she was a member of the Tissue Image Analytics (TIA) Laboratory. She has collaborated with several parties, including Coventry hospitals, where she collected most of the data and received her training in digital pathology. She is currently an Assistant Professor with Princess Nourah Bint Abdulrahman University, Riyadh, Saudi Arabia. She has published several articles in histology image analysis and has served as a reviewer for several journals.

SHAN E. AHMED RAZA received the Ph.D. degree in computer science from The University of Warwick, in 2014. He is currently an Associate Professor in computer science and is associated with the Applied Computing Division and the Tissue Image Analytics (TIA) Centre. Before joining The University of Warwick, he held a postdoctoral position for two years with the Institute of Cancer Research, U.K. He was worked on the lung TRACERx project funded by Cancer Research U.K. (CRUK). Prior to that, he worked for three years as a Research Fellow with the Computer Science Department, The University of Warwick, on a BBSRC-funded project exploring the origin of new beta cells during pregnancy. During his Ph.D. degree and postdoctoral roles, he also gained hands-on experience setting up experiments for the acquisition of images in wet biology laboratories and glass houses. His research interests include developing deep learning models for the analysis of microscopy images, integration of cancer imaging with genomics, and studying tumour microenvironment in the context of cancer evolution.

DAVID SNEAD is currently a Consultant Pathologist with the University Hospitals Coventry and Warwickshire (UHCW) and a Professor in pathology practice with The University of Warwick. He has been in post at Coventry for 20 years. He is also the Founding Director of PathLAKE, one of the five Innovate U.K. funded centers of excellence for the development of artificial intelligence in digital pathology and radiology. He is an international expert in the use of digital pathology having led Coventry to be one of the first hospitals in Europe, to switch to digital pathology for routine diagnosis. His team has published the world's largest validation study on the use of digital pathology, and which was awarded the 2016 Roger Cotton Prize for best paper in Histopathology. Prior to leading PathLAKE, he was with UHCW, for many years to the clinical lead for cellular pathology. This experience has given him a unique understanding of how innovative AI-based solutions can be deployed to address the major challenges facing cellular pathology department across the NHS.

NASIR M. RAJPOOT (Senior Member, IEEE) received the Ph.D. degree in computer science from The University of Warwick, in 2001. He is currently a Professor in computational pathology with The University of Warwick and an Honorary Scientist with the Department of Pathology, University Hospitals Coventry and Warwickshire (UHCW) NHS Trust. Prior to completing his Ph.D. degree, he was a Postgraduate Research Fellow with Yale University, USA, through the Applied Mathematics Program, from 1998 to 2000, and a Systems Engineering Fellow with the Pakistan Institute of Engineering and Applied Sciences (PIEAS), Pakistan, from 1994 to 1996. He has been the Director and the Founding Head of the Tissue Image Analytics (TIA) Laboratory, The University of Warwick, since 2012, and also the Co-Director of the recently funded B#15m PathLAKE Centre of Excellence on AI in Pathology, since January 2019. The focus of current research in the TIA Laboratory led by him is on developing novel computational pathology algorithms with applications to computer assisted grading of cancer and image-based markers for prediction of cancer progression and survival. He has been active in the digital pathology community for over a decade and has delivered over 50 invited and keynote talks, since 2015, at various national and international events and institutions. He is a member of the Association of the Computing Machinery (ACM), The British Association for Cancer Research (BACR), the European Association for Cancer Research (EACR), and the American Society of Clinical Oncology (ASCO). He was recently awarded the Wolfson Fellowship by the U.K. Royal Society and the Turing Fellowship by the Alan Turing Institute, the U.K.'s National Data Science Institute. He served as the President of the European Congress on Digital Pathology (ECDP), which took place at Warwick, in April 2019. Previously, he served as the General Chair for the U.K. Medical Image Understanding and Analysis (MIUA) Conference, in 2010, and the Technical Chair for the British Machine Vision Conference (BMVC), in 2007. He has been co-chaired several meetings in the histology image analysis (HIMA) series, since 2008, and served as a Founding PC Member for the SPIE Digital Pathology meeting, since 2012.